Supplementary information: A direct view at excess electrons in TiO_2 rutile and anatase

Martin Setvín,[1] Cesare Franchini,[2] Xianfeng Hao,[1] Michael Schmid,[1] Merzuk Kaltak,[2] Anderson Janotti,[3] Georg Kresse,[2] Chris G. Van de Walle,[3] and Ulrike Diebold[1]

[1]*Institute of Applied Physics, Vienna University of Technology, Wiedner Hauptstrasse 8-10/134, 1040 Vienna, Austria*

[2]*Faculty of Physics and Center for Computational Materials Science, Universität Wien, Sensengasse 8/12, A-1090 Wien, Austria*

[3]*Materials Department, University of California, Santa Barbara, CA 93106-5050*

I. EXPERIMENTAL AND COMPUTATIONAL METHODS

STM experiments were performed with an Omicron LT–STM head in a pressure below 1×10^{-9} Pa. A synthetic, polished rutile (110) sample and a natural, cleaved[1] anatase (101) sample were used. A detailed analysis of impurities in the anatase sample is given in ref. 2 The samples were cleaned in an adjoining preparation chamber by repeated 1 keV Ar^+ sputtering and annealing between 900 and 1000 K. Occasionally, heating in $p(O_2) = 5 \times 10^{-7}$ Pa, $T = 700$ K was performed. Electrochemically etched W tips were cleaned by Ar^+ sputtering, followed by a treatment on an Au (110) surface to a ensure metallic electronic structure of the tip. All STM images were measured in constant-height mode. The reasons are discussed below.

Point STS spectra were measured at open loop using a lock-in amplifier, with a modulation frequency of 764 Hz. The amplitude was 20 mV in Fig. 2 and 4 mV in Fig. 4. The set points and tip-sample distances for all data are given in Table S2. In Fig. 2, the noise near E_F was suppressed by the procedure suggested in Ref. 3. Spectra shown in Fig. 2 are averaged from 10 - 20 curves measured at different equivalent positions. The acquisition time for one spectrum was 20 - 40 s. Spectra in Fig. 4 consists of single spectra with an acquisition time of 90 s each. All STS measurements were repeated in at least 5 experimental sessions, using a different tip each time. The presented data were measured at 6 K in case of anatase and at 78 K in case of rutile, as stable tunneling conditions could not be achieved on rutile at very low temperatures. We have repeated the STS measurements presented in Fig. 2 in a wide temperature range (20 to 78 K for rutile and 6 to 150 K for anatase); no qualitative difference was observed in the behavior of the small polarons. The photoemission spectra (PES) in Fig. 2 were acquired at BESSY, beamline U49/2, endstation PHOENEXS, at room temperature. Both the rutile and anatase samples were mounted on the same sample holder to minimize any error in energy calibration. The PES spectra shown in Fig. 4 agree well with measurements in Ref. 4. The agreement in the peak energies in photoemission and STS indicates that the STS measurements are not affected by effects such as tip-induced band bending or charge transport limitations that can occur in low–temperature STS at semiconductor surfaces.[4]

The calculations are based on DFT within the generalized gradient approximation following the Perdew-Burke-Ernzerhof (PBE) parameterization as implemented in the Vienna Ab ini-

tio Simulation Package[5,6] (VASP). An effective on-site Hubbard U of 3.9 eV was introduced in order to treat the partially filled Ti d-shell and associated localization effects. This value of the on-site U was computed using the constrained random phase approximation (cRPA) within a maximall-localized Wannier functions basis including all Ti $3d$ states, as described in Ref. 7. The Wannier functions downfolding was done using the Wannier90 code[8] by means of the VASP2WANNIER90 interface.[9] We should emphasize that even with an accurate evaluation of U the DFT+U method remains an approximated parametric correction of standard DFT. This implies that a consistent account of different physical quantities such as bandgap, formation energies and polaronic properties is barely achievable using one single value of U[10–13].

The surface calculations were carried out using 2×4 and 1×4 supercells for rutile and anatase, respectively, with a slab thickness of 5 O-Ti-O trilayers. We included 15 Å of vacuum in order to isolate the two sides of the slab. Integration over the Brillouin zone was performed using the Gamma point only. The surface structure was optimized by including relaxation of the top 3 Ti-O trilayers, while keeping the central atoms in their ideal bulk positions and the bottom layers in positions corresponding to the relaxed, pristine surface. The dynamic behavior of the polarons was studied by means of FPMD (first–principles molecular dynamics) at a simulating temperature of 700 K for 10 ps, following the setup of Ref. 14. The formation of polarons in the bulk was studied by using 216- and 300-atom supercells for rutile and anatase respectively. The DFT+U derived relative stability of the most stable polaronic configurations as well as the polaronic stabilization and electronic energies were cross-checked through hybrid functional calculations using the screened hybrid functional of Heyd, Scuseria, and Ernzerhof.[15]

II. CLARIFICATION OF THE USED EXPRESSIONS

The theory of polarons and charge trapping is nowadays used in many fields of physics – for example in electrical conductivity, catalysis, high-temperature superconductivity, or polymer physics. As the development in these fields partially kept separate paths in the past, the terms 'polarons' or 'charge trapping' are often used in slightly different ways. Here we clarify how these are used in this work:

Polarons: A polaron consists of an electron coupled to surrounding lattice distortions. Here

we use the term 'polaron' only when the crystal lattice allows the self-trapping of electrons. This means that the polaron can exist in a perfect lattice (without any defects), it can move through the crystal.

Trapped electrons: In the case of the anatase surface with surface oxygen vacancies, the electrons stay localized at the vacancy and the perfect lattice does not allow small polaron formation. We call this configuration an 'electron trapped at a defect'.

Localized/delocalized electrons: By delocalized electrons, we mean electrons at the bottom of the conduction band that keep its band-like properties (k-dispersion). From this point of view, we can consider the shallow donor state in Nb-doped anatase as a delocalized electron, which is confined in space by the donor potential. On the other hand, small polarons in rutile or electrons trapped at V_Os in anatase are considered localized.

III. SURFACE STRUCTURE OF TiO_2 RUTILE (110) AND ANATASE(101)

Figures S1 a,b show standard (empty–states) STM images of TiO_2 rutile (110) and anatase (101), respectively. The structural models are discussed in detail in Ref. 16. From the shape of terraces in the large-scale image (inset in Fig. S1b) we distinguish the (inequivalent) $[\bar{1}01]$ and $[10\bar{1}]$ directions.[17]

IV. RUTILE(110) – EMPTY STATES IMAGES

In the main paper we mainly discussed electronic states within the band gap of the n-type semiconductor TiO_2, i.e., occupied states. The STS spectra in Fig. 2a clearly show that the rutile (110) surface has a surface state at $(+0.35 \pm 0.05)$ eV above the Fermi level. This surface state allows achieving atomic resolution in empty–states STM images. It is located mainly at Ti_{5c} atoms and at the oxygen vacancies. A small density of states is present at the oxygen atoms (see Fig. S2a). (We could resolve the oxygen atoms only at temperatures below 78 K; 25 K in case of Fig. S2.). The brightness of O atoms depends on their separation from oxygen vacancies; they appear brighter when the vacancies are close together.

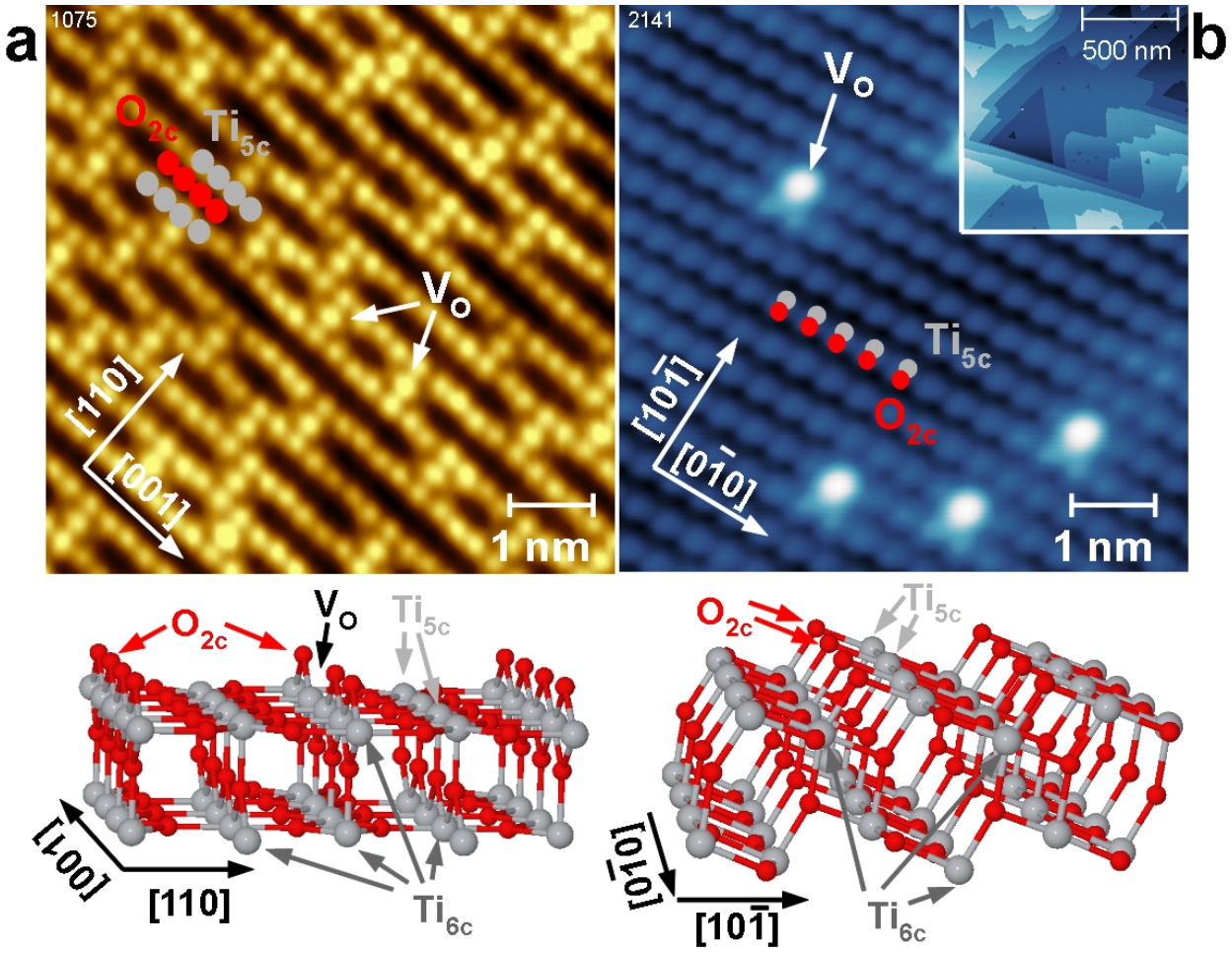

FIG. S1. **Structure of rutile (110) and anatase (101) surfaces.** a) STM image of rutile (110), $V_S = +0.6$ V, constant height mode, $T = 78$ K. Positions of surface 5–coordinated Ti atoms (Ti_{5C}) and 2–coordinated O atoms (O_{2C}) are marked, as well as a few surface O vacancies (V_O). b) STM image of the anatase (101) surface with a few surface V_O created by the STM tip.[2] $V_S = +0.8$ V, constant current mode, $T = 6$ K. The inset shows a large-scale image of the surface. Respective structural models are shown below the STM images.

V. STM MEASUREMENTS - DETAILS

STM and STS measurements of filled states of TiO_2 are difficult because of the low signal inherent in these measurements. As discussed below, we mainly resorted to the constant height mode for taking STM data. In the following we describe how we estimate the tip–sample (TS) distances in the experiment and compare it to the TS distances used in DFT calculations.

The starting point for estimating the experimental TS distances is the z position where the tip interacts strongly with the surface. It is known that approaching a tip to the region of

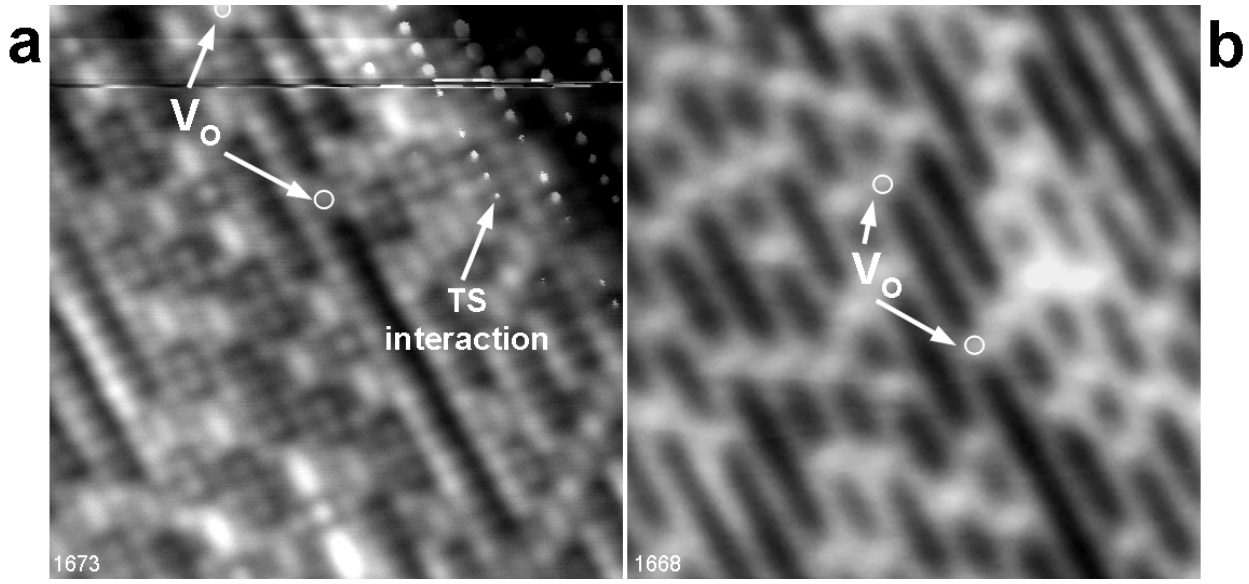

FIG. S2. **Empty–states STM images of rutile (110).** Shown are images taken at a) $V_S = +0.45$ V and b) $V_S = +0.8$ V and scanned with the same tip, i.e., no spontaneous tip changes occurred. Constant height images, $T = 25\ K$, $I_t \approx 0.25$ nA. The images are shifted because of thermal drift; circles mark equivalent positions. The image in (a) is used as a reference in Table S1.

short–range attractive forces with the surface atoms (for example covalent bonding) results in a significant modification of the tunneling current. This was first shown at the Si(111)-(7×7) surface by STM and DFT,[18] and later investigated in detail using non-contact atomic force microscopy.[19,20] Such modifications of the tunneling current are apparent in Fig. S2a. The tip interacts with O_{2c} atoms in the upper right corner, creating very localized, bright spots in the tunneling current. Oxygen typically forms bonds about 2 Å long and, according to AFM measurements, the modifications of the tunneling current usually occur at the onset of the chemical force. Consequently we estimate the TS distance in the reference image (Fig. S2a) as 2.5–3.0 Å. Measurements of $I(V)$, $I(z)$ and $z(V)$ dependencies then allow to estimate the TS distances in all other images.

Table S1 shows details of the scanning conditions and tip–sample distances used for the experiments discussed in the main text. Investigating the polarons in rutile requires close tip–sample distances, estimated as ≈ 3Å. The electrons trapped at the oxygen vacancies of anatase can be studied at ≈ 4.5 Å, which is comparable to regular scanning conditions. The shallow donor state in anatase was observed only at very close TS distances. The shallow state at ≈ −40 meV was very reproducible when measured with different tips. The tail

attributed to the phonon excitations[21] was strongly tip-dependent, however.

All presented STM images were measured in the constant (or quasiconstant) height mode. The information obtained from the constant height mode is essentially the same as from the constant current mode, which is used more commonly. However, the constant height mode turned out to be more suitable for imaging the filled states of TiO_2. The reasons are slightly different for anatase and rutile. For anatase, the filled-states LDOS is negligible anywhere except at the the V_Os. Thus using z–feedback in filled states would result in "tip crashes" on the clean surface. In rutile, the polarons hop across several lattice sites, thus the average LDOS is small. In addition, the polarons are preferentially located in the subsurface layer. Thus, for rutile, the TS distances are generally very small and the LDOS is mainly localized at the Ti_{5c} atoms. As the O_{2c} atoms protrude from the surface, using the constant current mode would result in an undesired approach of the tip to the protruding O_{2c} atoms.

The anatase STM images were measured in the constant height mode, while in case of rutile we mostly used the 'quasiconstant' mode, *i.e.* scanning with a very weak feedback loop. In this mode, the feedback keeps an almost constant height within each single line of the STM image (maintaining a z–corrugation at less than 5 pm per line) but strong enough to eliminate long–range effects such as thermal z–drift or plane tilting.

Table S2 shows all setpoints and estimated tip–sample distances for the STS measurements

TABLE S1. Estimated tip–sample distances in STM images and DFT calculations.

Rutile			
Figure number (file name)	V_S [V]	$\langle I_t \rangle$ [nA]	TS distance [Å]
S3a (1673) - reference	+0.45	0.28	2.5 - 3.0
1a (1177) - exp.	+1.0	1.0	3.3 - 3.8
1b (1181) - exp.	−0.6	0.2	2.5 - 3.0
1b (1180) - exp.	−1.4	0.2	2.8 - 3.3
4b - DFT	+1.0	—	3.0
4d - DFT	−1.0	—	3.0
Anatase			
Figure number (file name)	$V_S[V]$	$\langle I_t \rangle$ [nA]	TS distance [Å]
reference(not shown)	+0.1	0.5	2.5 - 3.0
1b(5697) - exp.	+0.8	6	3.8 - 4.3
1d(5697) - exp.	-1.0	1	3.8 - 4.3
4a - DFT	+1.0	—	4.0
4c - DFT	−1.0	—	4.0
5a(8425) - exp.	+0.3	0.25	2.9 - 3.4
5b(8425) - exp.	+0.3	0.05	2.9 - 3.4

TABLE S2. Setpoints and estimated tip–sample distances in STS measurements.

Figure number	V_S [V]	$\langle I_t \rangle$ [nA]	TS distance [Å]
2a - rutile	+0.7	0.2	3.0 - 3.5
2b - anatase	+1.5	0.25	4.5 - 5.0
5c - anatase	+0.2	0.25	2.7 - 3.2

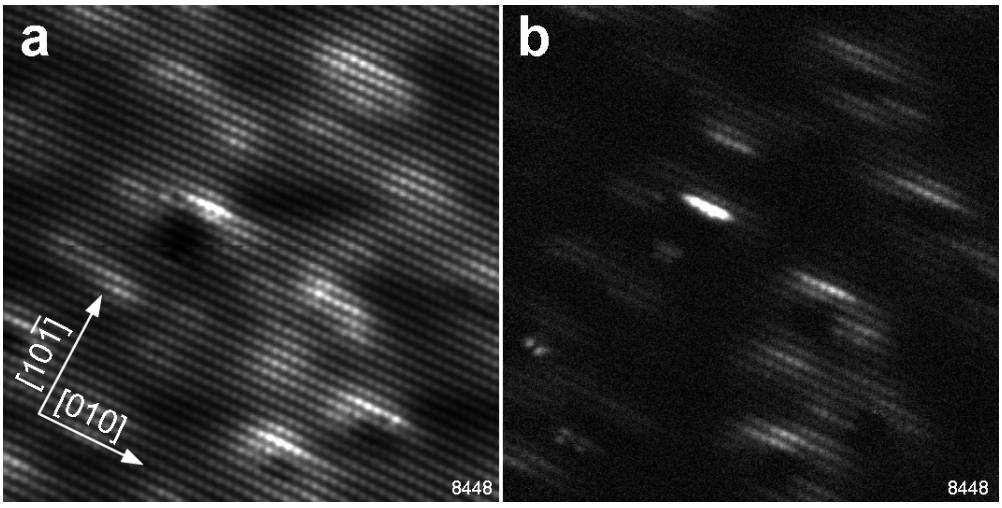

FIG. S3. **Shallow donor state on anatase (101).** Constant height STM images of anatase (101) measured at a) $V_S = +0.5$ V, b) $V_S = -0.5$ V. $T = 32$ K, 18×18 nm^2. The occupied density of states in (b) is extended along the [010] direction.

presented in the main text. STS of the electrons trapped at the anatase surface V_O is performed at much larger tip–sample distance than the STS of the shallow donor state. (For example, the data in Fig. 2h have been acquired under conditions where the shallow state is too weak to be observed.)

VI. SHALLOW DONOR STATES IN ANATASE

The STM images in Fig. 4 indicate a highly anisotropic shape of the occupied LDOS in the vicinity of subsurface donors; it is elongated along the [010] direction and shrunk along the perpendicular [10$\bar{1}$] direction. In STM images, the lateral extension of the occupied LDOS is somewhat dependent on the tip–sample distance; it appears larger when the tip is closer to the surface. The occupied LDOS also exhibits various shapes, likely because the dopants that it is bound to reside at different depths. Further, overlap of the potential from neighboring dopants often occurs, increasing the shape variance. Fig. S3 shows an example of a larger-scale STM image of the anatase(101) surface, containing several shallow donors.

From our experimental data we deduce the following:

a) The length along the [010] direction ranges from 12 to 25 Å.

b) The width in the $[10\bar{1}]$ direction ranges from 4 to 8 Å.

c) The ratio between the two directions lies between 2:1 and 5:1.

This peculiar anisotropic distribution of the electric charge originates from the intrinsic anisotropy of the dielectric properties of TiO_2[22,23] and can be rationalized and understood within the Fröhlich theory of large polarons.[24] The Fröhlich Hamiltonian depends on a single parameter, α, the electron-phonon interaction. It is defined as:

$$\alpha = \frac{1}{2}\left(\frac{1}{\epsilon_\infty} - \frac{1}{\epsilon_0}\right)\left(\frac{e}{\hbar\omega_0}\right)\left(\frac{2m\omega_0}{\hbar}\right)^{1/2} \approx 2\sqrt{m^*} \quad (1)$$

where ϵ_∞ and ϵ_0 are the high frequency and static dielectric constants, respectively, m^* the effective mass, and ω_0 the characteristic longitudinal optical phonon frequency. From the values of the α, m^*, and ω_0 along the [010] and $[10\bar{1}]$ directions taken from Ref. 22 we obtain $\alpha^{[010]} = 1.3$ and $\alpha^{[10\bar{1}]} = 3.7$, well within the intermediate electron-phonon coupling regime and in excellent agreement with quantum Monte Carlo calculations yielding an average of $\alpha = 2.5$ (Refs. 21 and 25).

In the intermediate electron-phonon regime the spatial extension of a large polaron is given by:

$$r_p = \frac{3}{0.44\alpha}\frac{1}{2}\left(\frac{\hbar}{2m_p\omega}\right)^{-1} \quad (2)$$

Here $m_p = m^*(1 + \alpha/6)$ represents the polaronic effective mass, which is again different along [010] and $[10\bar{1}]$, $m_p^{[010]} = 0.51$ and $m_p^{[10\bar{1}]} = 5.42$, respectively. By inserting these values in Eq. 2 we finally obtain $r_p^{[010]} = 19.0$ Å and $r_p^{[10\bar{1}]} = 3.5$ Å, in excellent agreement with the STM-derived values.

To further characterize the shallow donor state we have performed a DFT simulation on Nb-doped anatase. We used a large, 2×8 unit cell where one surface Ti_{6c} atom was substituted by Nb, as schematically shown in the inset of Fig. S4. The resulting STM simulation shows that the occupied LDOS is highly anisotropic (extended along [010] and quenched along $[10\bar{1}]$), and its intensity is modulated along the [010] direction with the intensity maximum near the donor center. The DFT calculation shows that the delocalized solution is only obtained after relaxation of the lattice, while an unrelaxed lattice results in the electron localization

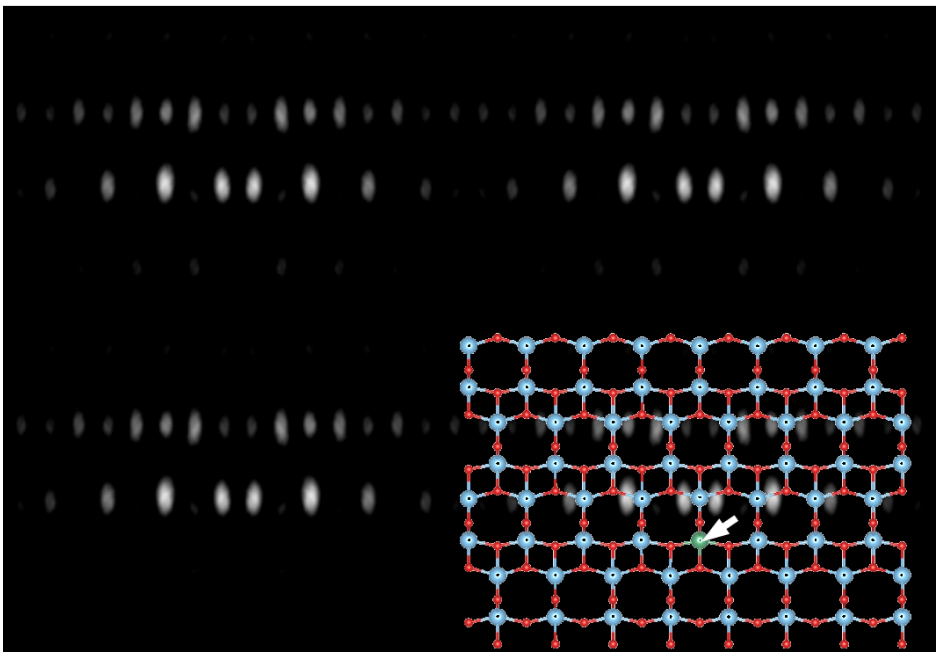

FIG. S4. **DFT calculation of a subsurface Nb-dopant** Simulated, occupied states (≈ -0.1 eV) STM image of Nb-doped anatase in 'constant-height' mode at about 3.2 Å above the surface. A (2×8) unit cell was used for the calculation (multiplied here by 2×2). The Nb dopant is marked by arrow.

at the Nb dopant. The lattice relaxations around the Nb dopant are significantly smaller (below 0.06 Å) than in the material doped by oxygen vacancies (0.1 to 0.15 Å). On the other hand, the relaxations around the Nb dopant extend to further distances.

In the main text, we show a map of normalized conductance (dI/dV)/(I/V) measured above the shallow donor state in Fig. 4. The corresponding raw dI/dV data are shown in Fig. S5. The spectroscopic trace we have observed above the subsurface Nb dopants is essentially identical to the ARPES measurements performed by Moser *et al* in Ref. 21: Both the main peak at 40 meV below the Fermi level and the tail attributed to electron–phonon interactions. However, the measurements reported in Ref. 21 were performed on anatase doped by beam-induced oxygen vacancies. Our STS experiments show that oxygen vacancies provide trapped electrons (deep stats); this controversy requires a clarification. The data in Ref. 21 were measured on the anatase (001) plane, which is (4×1) reconstructed. It is likely that the oxygen vacancies on this surface provide delocalized electrons (because of a different strain and lattice relaxations than on the (101) plane). The large polaron is a 3-dimensional object and its properties are determined by the anatase crystal lattice rather than the dopant type. Thus it is not surprising that our data closely resemble the ARPES

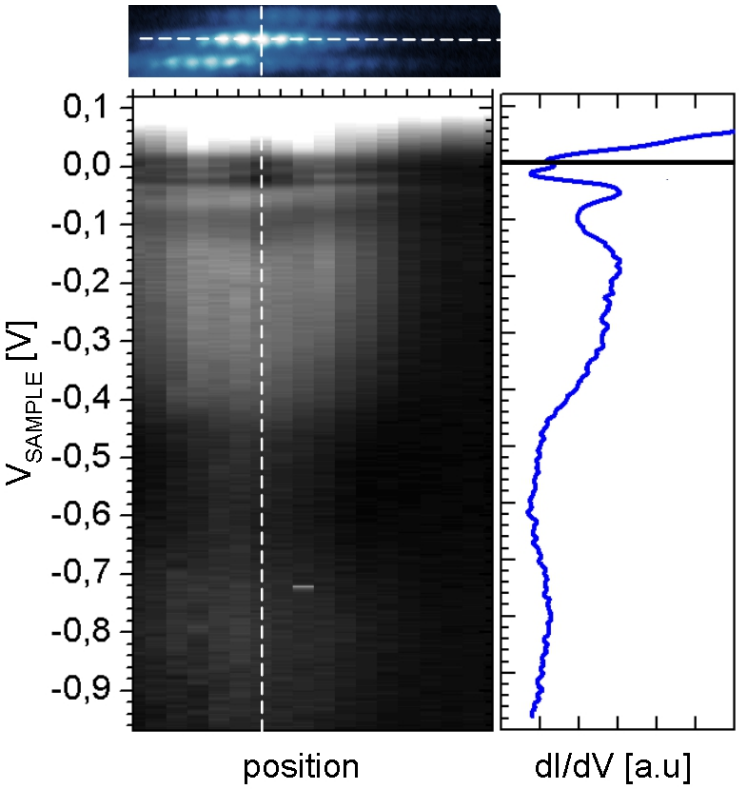

FIG. S5. **Raw STS data measured in vicinity of a subsurface donor.** A map of dI/dV measured at different points along the dashed line in the image.

measurements,[21] even though the crystal plane and the dopant are different.

VII. STM MEASUREMENTS OF POLARONS - TIME SCALES

As mentioned in the main text, in fast spectroscopies, where excitations occur at time scales shorter than those characteristic for phonons, polarons show signatures of their trapped state (E_{EL} in Fig. 1). This raises the issues of time scales in our STM and STS measurements. Tunneling is inherently a fast process. Each possible trapping center can only contain only one electron. In our measurements we typically use tunneling currents of the order of 10 to 100 pA. Thus 10^8 electrons per second are removed from each site. In order to observe the signature of polarons in an STM or STS measurement, the electrons in the trapping center must be replenished at a higher rate, and each polaron must have time to relax in its equilibrium position. The capture rate for forming a polaron at a particular site, R is given by $R = C * n$, with a typical capture coefficient C in the range from 10^{-8} to 10^{-6} $\mathrm{cm^3 s^{-1}}$, and n the concentration of electrons.

Our anatase sample is doped with 1.1% Nb, thus the electron concentration n is estimated as 3×10^{20} cm^{-3}. This results in electron trapping rate R of the order of $10^{13\pm1}$ s^{-1}, at least three orders of magnitude faster than the rate of electron tunneling. At a typical phonon frequency of ps, the polaronic state always has enough time to relax between single tunneling events.

For slightly-reduced rutile,[26] typical values of n are of the order 10^{19} cm^{-3}, still yielding capture rates that are well above the tunneling rate in our STM measurements. It should be noted, however, that the STM experiments on rutile were only possible for temperatures in excess of ≈20 K; likely they were limited by the hopping rate of polarons at low temperatures.

[1] O. Dulub and U. Diebold, J. Phys. Cond. Matt. **22**, 084014 (2010).

[2] M. Setvin, U. Aschauer, P. Scheiber, Y.-F. Li, *et al.*, Science **341**, 988 (2013).

[3] M. Prietsch, A. Samsavar, and R. Luedke, Phys. Rev. B **40**, 11850 (1991).

[4] J. Myslivecek *et al.*, Phys. Rev. B **73**, 161302 (2006).

[5] G. Kresse and J. Furthmüller, Phys. Rev. B **54**, 11169 (1996).

[6] G. Kresse and D. Joubert, Phys. Rev. B **59**, 1758 (1999).

[7] Y. Nomura, M. Kaltak, C. Taranto, S. Sakai, A. Toshi, R. Arita, K. Held, G. Kresse, and M. Imada, Phys. Rev. B **86**, 085117 (2012).

[8] A. A. Mostofi, J. R. Yates, Y.-S. Lee, I. Souza, D. Vanderbilt, and N. Marzari, Comp. Phys. Comm. **178**, 685 (2008).

[9] C. Franchini, R. Kovacik, S. S. Murphy, J. He, C. Ederer, and G. Kresse, J. Phys. Cond. Matt. **24**, 235602 (2012).

[10] N. A. Deskins and M. Dupuis, Phys. Rev. B **75**, 195212 (2007).

[11] H. Cheng and A. Selloni, J. Chem. Phys. **131**, 054703 (2009).

[12] E. Finazzi, C. D. Valentin, G. Pacchioni, and A. Selloni, J. Chem. Phys. **129**, 154113 (2008).

[13] S. Chretien and H. Metiu, J. Phys. Chem. C **115**, 4696 (2011).

[14] P. M. Kowalski, M. F. Camellone, N. N. Nair, B. Meyer, and D. Marx, Phys. Rev. Lett. **105**, 146405 (2010).

[15] J. Heyd, G. E. Scuseria, and M. Ernzenhof, J. Chem. Phys. **118**, 8207 (2003).

[16] U. Diebold, Surf. Sci. Rep. **48**, 53 (2003).

[17] X.-Q. Gong, A. Selloni, M. Batzill, and U. Diebold, Nat. Materials **5**, 665 (2006).

[18] P. Jelinek, M. Svec, P. Pou, R. Perez, and V. Chab, Phys. Rev. Lett. **101**, 176101 (2008).

[19] Y. Sugimoto, I. Yi, K. Morita, M. Abe, and S. Morita, Appl. Phys. Lett. **96**, 263114 (2010).

[20] Z. Majzik, M. Setvín, A. Bettac, A. Feltz, V. Cháb, and P. Jelinek, Beilstein J. Nanotech. **3**, 249 (2012).

[21] S. Moser *et al.*, Phys. Rev. Lett. **110**, 196403 (2013).

[22] M. Dou and C. Persson, J. Appl. Phys. **113**, 083703 (2013).

[23] L. Chiodo, J. M. Garcia-Lastra, A. Iacomino, S. Ossicini, *et al.*, Phys. Rev. B **82**, 045207 (2010).

[24] H. Frhlich, Adv. Phys. **3**, 325 (1954).

[25] A. S. Mishchenko, N. V. Prokofev, A. Sakamoto, and B. V. Svistunov, Phys. Rev. B **62**, 6317 (2000).

[26] E. Yagi, R. Hasiguti, and M. Aono, Phys. Rev. B **54**, 7945 (1996).